Eur. Phys. J. E (2007)
DOI: 10.1140/epje/e2007-00031-0

THE EUROPEAN PHYSICAL JOURNAL E

The influence of grain shape, friction and cohesion on granular compaction dynamics

N. Vandewalle[1,a], G. Lumay[1], O. Gerasimov[1,2], and F. Ludewig[1]

[1] GRASP, Physics Department, University of Liège, 4000 Liège, Belgium
[2] Department of General and Theoretical Physics, Odessa State University of environment, Ukraine

Received 1st November 2006 / Received in final form 15 February 2007
Published online: 30 March 2007 – © EDP Sciences, Società Italiana di Fisica, Springer-Verlag 2007

Abstract. This article is a review of our recent and new experimental works on granular compaction. The effects of various microscopic parameters on the compaction dynamics are addressed, in particular the influence of the grain shape, the friction and the cohesion between the grains. Two dimensionnal and three dimensionnal systems are analysed. And the role of dimensionality will be emphasized. Theoretical and numerical investigations provide additional informations about that phenomenon. Indeed numerical models permit us to study the influence of some parameters not easily accessible experimentally. Our results show that the above mentioned parameters have a deep impact on the compaction dynamics. Anisotropic grains lead to two different compaction regimes separated by a "burst" of the packing fraction. Friction is observed to modify how the grains are arranged in the pile. This is confirmed by numerical simulations. Cohesive forces between particles inhibit compaction and lead to extremely low values of the packing fraction.

PACS. 45.70.-n Granular systems – 45.70.Cc Static sandpiles; granular compaction

1 Introduction

The complex collective behaviors of an assembly of particles is due to the dissipative nature of the inter-particle forces. A wide variety of phenomena can be observed by varying the strength of power supply to a granular system. A low power input may induce slow relaxation in a series of metastable states or an intermittent collective motion, while a steady state results from a large enough energy supply.

When a pile of granular material is gently shaked, the packing fraction of the pile slowly increases. This phenomenon is called granular compaction. Despite numerous studies devoted to granular compaction kinetics and associated quasistatic properties of granular packings [1–8], the physical understanding of those phenomena in many senses poses a serious challenge to physicists. Indeed, the complexity results in the observation of a myriad different states either metastable or even quasistationnary whose appearance escorts the extremely slow dynamics of compaction. Moreover, the way a packing finds its way to a denser system is strongly influenced by the preparation of the studied sample, the experimentally accessible time scales, the way of shaking, the existence of memory effects, etc. And those dependences are naturally supplemented by gravity, inelasticity, friction, cohesion and dispersion of the particles.

[a] e-mail: nvandewalle@ulg.ac.be

One should note that the knowledge of granular material properties, and in particular compaction dynamics [9], has a major economical impact on all industries, as granular materials are the second most manipulated material in industry behind liquid water.

This paper reports our recent and new experiments, underlining the various aspects of a complex compaction dynamics. Our analysis provides evidences for a different packing dynamical regimes as a function of various parameters. We will discuss 2D and 3D experimental results obtained with cylindrical and spherical millimetric grains. We will investigate the influence of the friction and of the cohesion between grains on the compaction dynamics. The case of powders will be also envisaged. Numerical approaches will also be discussed in order to check for various effects.

2 State of the art

2.1 Compaction laws

Over the last decade, lots of works [1–7,9–13] has been done in the field of granular compaction. It has been proposed by Knight et al. [1], that the packing fraction η of a pile submitted to a series of identical taps obeys an inverse logarithmic law

$$\eta(n) = \eta_\infty - \frac{\eta_\infty - \eta_0}{1 + B\ln(1 + \frac{n}{\tau})}, \qquad (1)$$

where B and τ are dimensionless parameters. The parameters η_0 and η_∞ are respectively the initial and the final packing fraction. The dynamical parameters B and τ are strongly correlated. Therefore, we fix the parameter B to unity in the next sections. The inverse logarithmic law 1 was also obtained in simple numerical models like the Tetris one [7]. The law (1) could also be derived from theoretical arguments [10]. Some of the arguments will be discussed below.

More recently, Philippe and Bideau [4] found that the compaction dynamics is better fitted by a stretched exponential law, like

$$\eta(n) = \eta_\infty - (\eta_\infty - \eta_0) \exp\left[-\left(\frac{n}{\tau}\right)^\beta\right]. \quad (2)$$

This stretched exponential law has the great advantage to fit a saturation of the packing fraction which is sometimes accessible in experiments (for large n values). Both parameters τ and β correspond respectively to a characteristic tap number and to a stretching exponent $0 \leq \beta \leq 1$. One should notice that in the experiments of Philippe and Bideau, the steady state corresponds to a dynamical balance between convection and compaction. This is not always the case in other experiments. For a review of their results, see reference [3]. This stretched exponential law (2) has been recently confirmed [11] in our 2D experiments (see also Sect. 3). However, in these experiments, the steady state corresponds to a crystallization of the pile.

Logarithmic and stretched exponential laws look similar but fit differently the experimental data. Both scenarii seem to be mixed in real experiments. The next subsection explains that both laws are also intimately linked in simple kinetics theories.

2.2 Free volume kinetic model

In order to model compaction, a free volume theory [10] is often proposed. In this framework, one can describe the process where the solid particle (associated with the grain) with volume ω can jump into a hole of the appropriate size Ω distributed in their own with a certain distribution function $f(\omega/\Omega)$. The simplest rate equation which describes such a free volume kinetics takes a form

$$\frac{d\eta}{dn} = kf \quad (3)$$

where the variable η is the packing fraction, and k is a kinetic coefficient. Introducing the limiting maximum values for the compactivity η_m and estimating the simplest Poisson distribution for the free volume

$$\Omega = \omega\left(\frac{1}{\eta} - \frac{1}{\eta_m}\right) \quad (4)$$

one has

$$\frac{d\eta}{dn} = k \exp\left(-\frac{\eta_m \eta}{\eta_m - \eta}\right). \quad (5)$$

Rigorous analytical solution of this equation which connects the packing fraction η with the number of taps n can be obtained in the following functional form

$$(\eta_m - \eta_1) \exp\left(\frac{\eta_m^2}{\eta_m - \eta_1}\right) + \eta^2 E_1\left(-\frac{\eta_m^2}{\eta_m - \eta_1}\right) - (\eta_m - \eta) \exp\left(\frac{\eta_m^2}{\eta_m - \eta}\right) - \eta_m^2 E_1\left(-\frac{\eta_m^2}{\eta_m - \eta}\right) = k \exp(\eta_m) n \quad (6)$$

where η_1 is the initial compactivity and $E_1(z)$ is an integral exponent [26]. If the initial state is already densified, i.e. $\eta_1 \to \eta_m$ $\left(\frac{\eta_m^2}{\eta_m - \eta_1} \gg 1, \frac{\eta_m^2}{\eta_m - \eta} \gg 1\right)$ equation (6) gives

$$\eta = \eta_m - \frac{\eta_m^2}{\ln \gamma + \ln\left(\frac{a}{\gamma} + n\right)} \quad (7)$$

where $a = |(\eta_m - \eta_1) \exp(\frac{\eta_m^2}{\eta_m - \eta_1}) + \eta_m^2 E_1(-\frac{\eta_m^2}{\eta_m - \eta_1})|$ and $\gamma = k \exp(\eta_m)$. This logarithmic law for granular compaction has been many times reported either by experimentalists or by theoreticians [1,10] (see Eq. (1)). When the system is initially diluted so that $\eta_m^2/(\eta_m - \eta_1) < 1$ and $\eta_m^2/(\eta_m - \eta) < 1$, from (6) we perform

$$\eta = \eta_1 + \gamma n, \quad (8)$$

i.e. much faster than a logarithmic behavior.

One should note that when $\eta_m^2/(\eta_m - \eta_1) < 1$ but $\eta_m^2/(\eta_m - \eta) > 1$, from (6) we derive again the logarithmic law, given by (7). Independently from how the system was initially prepared (diluted or densified), in the limit when η tends to η_m, the model gives the slow logarithm rate of η growth.

This simple argumentation demonstrates the principal possibility of getting different kinetic scenarii, i.e. logarithmic dynamics and more faster stages, of compaction already being in the framework of a mean-field arguments, included in the origin of free volume kinetic model. Different scenarii are found in experiments and a mixture of those dynamics is more appropriate for describing the experimental data. This will be discussed in the next sections.

3 Experimental approach

3.1 Experimental set-up

A container filled with a few thousands of spherical (Figs. 1a and 1b) or cylindrical (Figs. 1c and 1d) grains is placed above an electromagnetic hammer. Ceramic, glass and lead beads have been tested. In order to vary the friction between grains, we used different ceramic beads with similar sizes and shapes but different surface properties. The compaction dynamics of pharmaceutical powders will

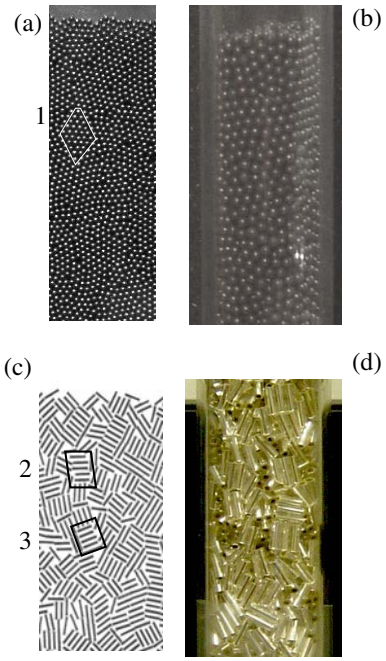

Fig. 1. Pictures of the different piles studied in our compaction experiments. The pictures (a) and (c) correspond respectively to snapshots of a pile of spheres and a pile of cylinders in a 2D geometry. The pictures (b) and (d) correspond to the 3D geometry. These snapshots have been recorded in the middle of the compaction process. Hexagonal structures are observed in region 1. Domains of aligned grains and domains of ideally ordered grains are observed respectively in regions 2 and 3.

Table 1. Summary of the grain characteristics (average size and polydispersity) in our experiments.

	Size	Polydispersity
Spherical lead beads	$d = 2.4$ mm	3.6%
Spherical ceramic beads	$d = 1.8$ mm	15%
Glass rods	$d = 2.16$ mm	3%
	$\ell = 6.73$ mm	
Powder (Avicel)	$d = 50$ μm	Strong

be also analyzed (Fig. 3). Table 1 summarizes the main characteristics of the grains we used in our experiments.

For granular systems, different containers allow us to investigate either 2D (Figs. 1a and 1c) or 3D (Figs. 1b and 1d) systems. The 2D container corresponds to two vertical glass plates separated by one grain diameter [11]. In this geometry, the motion of every grain can be optically tracked. The 3D container is a cylindrical tube with a diameter fifteen times larger than a grain diameter [13].

One should remark that our experimental set-up is different from usual ones which generally use an oscillating system to produce the series of taps. However, in our set-up, an electromagnetic hammer is placed below the container for tapping. The motion of the container during a tap is very limited with an amplitude around 0.3 mm. The hammer produces a shock wave in the pile, starting at the bottom of the pile and going upward. The main acceleration peak lasts 0.25 ms and the maximum intensity

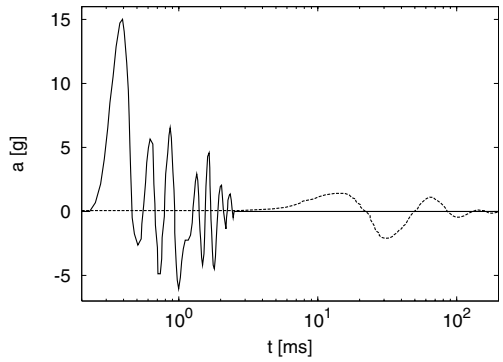

Fig. 2. Log-scale plot of the acceleration experienced by the container in our system during a tap (plain line) and the acceleration experienced by the system in the Rennes experiments (dashed line) [25]. Our container undergoes a short peak of acceleration. The width of the main peak is 0.25 ms and the maximum intensity is 15 g. Some damped oscillations are observed during a few milliseconds. For the Rennes experiment, the width of the main peak is 25 ms and the acceleration is much lower.

reaches 15 g. With this shaking method, we do not observe any convection in the pile. In Figure 2, we compare the tapping system of Philippe and Bideau [4,5] and our system through the signals from an accelerometer placed on both containers. We observe a clear difference between both methods: the associated time scales are different. The intensity, the number and the frequency of the taps can be controlled. The "density" or packing fraction η of the system is measured through the vertical position of the upper grains in the container. Our experimental set-up has been precisely reported in [12,11] for 2D experiments and in [13] for 3D experiments.

In a second part of our experiments, we have studied the influence of the cohesion between the grains on the compaction dynamics. For that study, we used a common pharmaceutical powder: lactose grains (Avicel). The typical size of the grains is 50 μm. Moreover, the grains are anisotropic objects (see Fig. 3). In order to modify the cohesion between the grains, we added a small (0.5%) amount of Aerosil. The Aerosil is a powder made of nano-particles, commonly used in pharmaceutical industries to increase the flowability of a lactose system. Indeed, after mixing, these nano-particles are situated at the surface of Avicel grains. They decrease the Van der Waals interactions between those grains. In this study of powders, we produced only a few thousands of taps. Indeed, after this number of taps, the system becomes a brittle pellet. We performed the powder compaction experiments only in the 3D cylindrical container.

3.2 Compaction curves

Typical compaction curves $\eta(n)$ are presented in Figure 4 for spherical lead beads and in Figure 5 for cylindrical grains. The curves on both Figures 4 and 5 underline the different behaviors we expect from 2D and 3D situations.

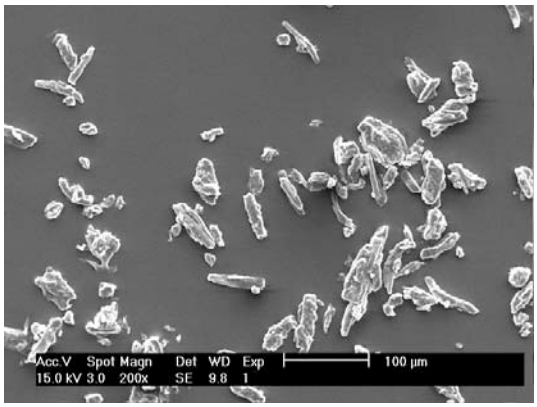

Fig. 3. SEM micrograph of lactose avicel grains. This picture reveals the anisotropic nature of those grains. Picture taken by Bodson [9].

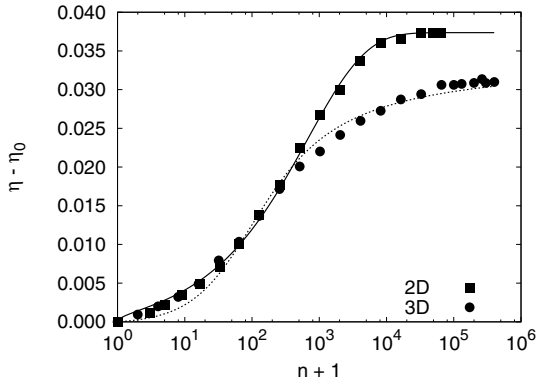

Fig. 4. Two compaction curves $\eta(n)$ for lead spherical beads placed onto an electromagnetic hammer. Both cases correspond respectively to 2D and 3D situations. We substract the initial packing fraction η_0 in order to obtain curves starting from the same point. The 2D data are fitted by the stretched exponential law (2). The 3D data are better fitted by the inverse logarithmic law (1).

Table 2. Summary of the different parameters obtained from the compaction curves presented in Figures 4 and 5.

	Spherical grains	Cylindrical grains
2D	$\eta_0 = 0.825$, $\eta_\infty = 0.862$	$\eta_0 = 0.775$, $\eta_\infty = 0.877$
	$\Delta\eta = 0.037$	$\Delta\eta = 0.102$
3D	$\eta_0 = 0.560$, $\eta_\infty = 0.595$	$\eta_0 = 0.546$, $\eta_\infty = 0.738$
	$\Delta\eta = 0.035$	$\Delta\eta = 0.192$

The parameters extracted from these compaction curves are summarized in Table 2.

For spherical particles, the 2D case exhibits a fast compaction kinetics since the data is nearly approached by a stretched exponential law (2), as suggested by recent works [4,11]. This stretched exponential law can be explained by the presence of crystallization during the compaction process in the 2D pile [11]. Indeed, we observe some domains of hexagonally packed grains (see region 1 in Fig. 1a). These domains grows during the compaction process [11]. At the end of the process, nearly all the grains are hexagonally packed in the container. The final packing

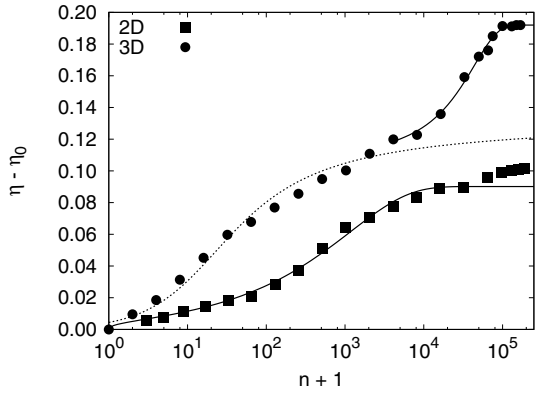

Fig. 5. Two compaction curves $\eta(n)$ for glass cylindrical grains placed onto an electromagnetic hammer. Both cases correspond respectively to 2D and 3D configurations. We substract the initial packing fraction η_0 in order to obtain curves starting from the same point. The first stage of the curve corresponding to the 2D case is fitted by a stretched exponential law (2). The first stage of the 3D curve is better fitted by the inverse logarithmic law (1). The second stage of the 3D curve is fitted by a stretched exponential law (2).

fraction $\eta_\infty \approx 0.862$ is still lower than the hexagonal packing fraction $\eta_h \simeq 0.91$. This is explained by the presence of frozen defects in the packing. The growth of hexagonal domains in the pile can be modeled by the Avrami model of crystallization [11]. This model assumes an exponent $\beta = 0.5$ in the 2D geometry. One should note that, in the experiments in Rennes [4,5], the exponential saturation of the density is due to a competition between compaction and convection. This competition induces a clear saturation of the density at the end of the process. In our experiment, the steady state is mainly due to the crystallization. Therefore, we obtain the same stretched exponential law but the mechanisms explaining this law could have different origins.

The 3D pile of spherical grains exhibits a much slower compaction kinetics than the 2D case. This curve is better fitted by an inverse logarithmic law (1) proposed by independent studies [1,2]. The parameter B is fixed to unity in order to have only two free fitting parameters: τ and η_∞. The 3D case is fundamentally different from the 2D case since crystallization is far to be observed in the bulk, even if the grains situated near the walls seems to be ideally ordered. Indeed, both values of the initial η_0 and final packing fraction η_∞ are much lower than the random close packed limit $\eta_{RCP} \simeq 0.64$.

With cylindrical particles, the compaction dynamics is more complicated. We observe two successive stages in the compaction process (see Fig. 5). An exponential saturation is followed by a jump of the packing fraction. The presence of two stages can be explained by the analysis of the grain organization. In the 2D pile, we observe some domains of aligned grains (see region 2 in Fig. 1c) and some domains of aligned and ordered grains (see region 3 in Fig. 1c). In the first part of the compaction process, the domains of aligned grains are growing [12]. At the end of the compaction process, these domains are sheared to form

aligned and ordered domains. Those mechanisms give rise to two successive stages in the compaction dynamics.

The compaction dynamics of the 3D pile of cylindrical particles exhibits also two successive stages (see Fig. 5). This particular compaction dynamics has been also observed by Villaruel et al. [14]. The presence of two stages is clearly explained by a transition between a disordered initial state and a "nematic" final state. Indeed, at the beginning of the compaction process, the pile is completely disordered. After a few thousands of taps, the grains started to align themselves along the vertical direction. The first compaction stage is fitted by an inverse logarithmic law (1). At the end of the second compaction stage, we observe a clear saturation of the density η. This saturation is better fitted by a stretched exponential law.

From these observations, we can draw a general conclusion about the compaction dynamics. When some crystallization is observed inside the bulk, the compaction dynamics is better fitted by a stretched exponential law (2). Otherwise, the compaction dynamics is logarithmic.

3.3 The role of friction

The great majority of studies on compaction dynamics considered the geometry of the grains and the level of disorder in the packing. The role of microscopic physical parameters such as friction, deformation, inelasticity and cohesion has rarely been treated experimentally.

Two kinds of polydisperse ceramic beads were studied. They are characterized by different surface roughness values. Except this particular difference, grains are identical in size distribution, shape, weight, etc. Those grains are considered below as "smooth" and "rough" beads. Beads are placed in the 3D container (vertical tube). The compaction experiments have been repeated five times for both types of grains. The compaction curves for both surface properties are presented in Figure 6. Table 3 summarizes the data extracted from these compaction curves. The high packing fraction values ($0.586 < \eta < 0.648$) measured in the system are explained by the high polydispersity (15%) of the grains. Both compaction curves are fitted by the inverse logarithmic law (1). We observe a relevant difference of packing fraction between "rough" and "smooth" particles. Indeed, both initial η_0 and final packing fractions η_∞ have larger values for "smooth" particles. This difference means that "smooth" grains are able to find a better organization (a grain arrangement that minimizes the local potential energy) than the rough particles. However, the characteristic time τ has almost the same value within error bars. Friction does not seem to affect the compaction dynamics. That experimental result was unexpected.

3.4 The role of cohesion (for powders)

The flow properties of a powder composed by microscopic grains are quite different from the case of granular materials made of millimetric grains [15]. This difference is due

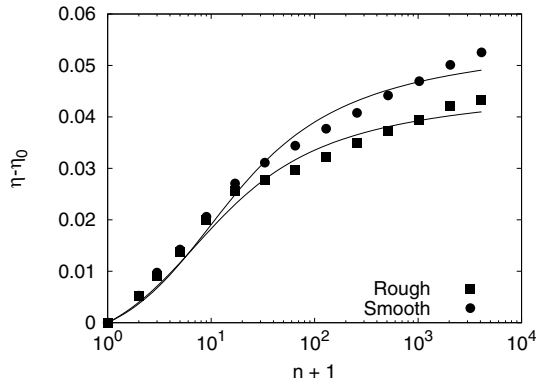

Fig. 6. Two typical compaction curves proving the important role of friction. Indeed, both experiments are done with either smooth or rough identical ceramics beads. We substract the initial packing fraction η_0 in order to obtain curves starting from the same point. Both curves are fitted by the inverse logarithmic law (1).

Table 3. Summary of the parameters extracted from compaction curves of "rough" and "smooth" ceramic beads.

"Rough"	"Smooth"
$\eta_0 = 0.586$	$\eta_0 = 0.594$
$\eta_\infty = 0.634$	$\eta_\infty = 0.651$
$\tau = 11 \pm 2$	$\tau = 14 \pm 2$

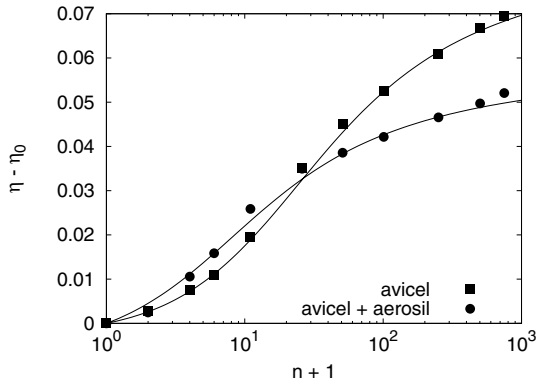

Fig. 7. Two compaction curves proving the important role of cohesion. We substract the initial packing fraction η_0 in order to obtain curves starting from the same point. Both curves are fitted by the inverse logarithmic law (1).

to the Van der Waals interactions between the grains in the powder. In this section, we study the influence of this cohesion on the compaction dynamics.

Two kinds of powders are studied which are characterized by different cohesive forces between the grains. The first compaction experiment has been performed with a cohesive lactose powder (Avicel). The second one has been made with the same powder and a small amount (0.5%) of Aerosil. The presence of Aerosil reduces drastically the Van der Waals interactions between the grains. Figure 7 presents both compaction curves. The inverse logarithmic law (1) fits correctly both compaction curves. The parameters extracted from the fits are presented in Table 4.

Table 4. Summary of the parameters extracted from the fit of both compaction curves of powder presented in Figure 7.

Avicel	Avicel + Aerosil
$\eta_0 = 0.224$	$\eta_0 = 0.248$
$\eta_\infty = 0.314$	$\eta_\infty = 0.310$
$\tau = 32 \pm 2$	$\tau = 12 \pm 2$

For both powders, the packing fraction is lower than the packing fraction of a pile of millimetric grains. Moreover, when the cohesion between the grains increases, the initial packing fraction η_0 decreases. The variation of the packing fraction $\eta_\infty - \eta_0$ increases also with cohesion. The major difference between both curves is observed in the compaction dynamics. Indeed, the characteristic time τ varies strongly with the cohesion. This characteristic time is shortens when the cohesion decreases.

4 Numerical approach

Because of the complexity of compaction experiments and some limitations of theoretical approaches, numerical models have been elaborated in order to reproduce compaction. Earlier models, like "Tetris-like" models, were computed on lattices [7]. Those probabilistic models [8], i.e. including randomness in the grain motions, reproduce the logarithmic law (1) proposed in the first experimental studies. More recently, off-lattice models have been also developed [16,17]. The off-lattice models or DEM (Discrete Element Method), which are deterministic ones, lead also to the logarithmic compaction law (1). One of the major advantages of the numerical studies is the possibility to control some physical parameters, including microscopic properties of grains like friction. The latter are often not experimentally accessible.

In this section, a numerical work about the influence of friction on the compaction kinetics is reported. Several works have already approached the problem of friction in granular materials [18], some of them for stress propagation [19]. For example, the properties of static piles composed by spheres versus the friction has been studied earlier [20]. However, the influence of friction on the compaction dynamics is less known, even though "Tetris-like" models [8,21] have been recently proposed for that purpose.

4.1 Numerical model

The numerical model we developed is a DEM-based model which considers Non-Smooth Contact Dynamics (NSCD) used for granular problems [22,23]. The NSCD builds a link between all forces in the pile and the grain motions through the Newton's equations. For a complete determination of all force values, the model is based on the Signorini-Coulomb diagrams, which are non-smooth in opposition to the case of Molecular Dynamics (MD) as presented in Figure 8.

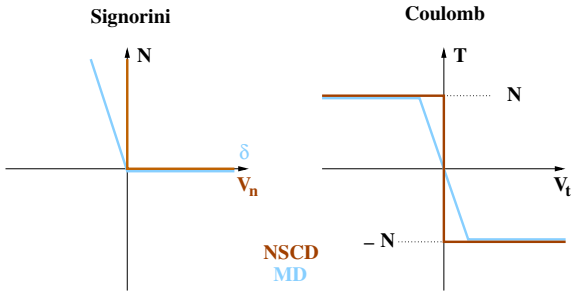

Fig. 8. (Left) Signorini diagram which links the normal force N to the overlap δ between two grains (MD, in dark grey) or to the relative normal velocity v_n (NSCD, in light grey). (Right) Coulomb diagram which links the tangential force T to the relative tangential velocity v_t by projection on the extreme values $\pm\mu N$.

The model supposes that the grains are solid particles and that the contacts are of punctual nature. In molecular dynamics (MD), each contact is computed alone and a contact force is evaluated from the overlap δ between grains (see the Signorini diagram of Fig. 8). The MD characteristic time is the collision time. In opposition, all contacts in NSCD are computed simultaneously and the model makes a complete stress network in the pile, at each time step. The grain overlap δ is never considered in the force calculation. The characteristic time is thus associated with the motion of the grains. The NSCD simulations are thus more efficient than MD ones for modeling long relaxation times.

For all numerical simulations in this work, the piles were prepared by a gravitational deposition (rain-like) of the grains. The grains are first placed on a virtual 2D random lattice with random velocities, before relaxing until a stable position has been reached. The taps are realized though a sinusoidal vertical motion of the container over one period; i.e.

$$z = A\sin(\omega t + \phi) \tag{9}$$

where $\omega = 2\pi f$, $\phi = -\pi/2$. The amplitude and frequency are linked to the reduced acceleration Γ:

$$\Gamma = \frac{A\omega^2}{g}. \tag{10}$$

In this work, all simulations are realized for $f = 32\,\mathrm{Hz}$ and $\Gamma = 6$. The time between two successive taps is taken larger than the relaxation time associated to the pile. It should be noted that those conditions are close to the ones of the Rennes experiment.

4.2 The effect of friction

In opposition to the experimental works described above, the numerical simulations allow to control exactly the friction coefficient between the grains. Borders have been first considered in the simulations in order to estimate the effect of wall friction. For high values of the friction coefficient, two convection cells appear as shown in Figure 9.

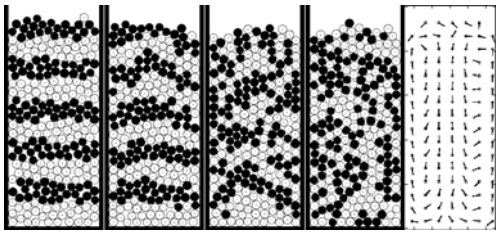

Fig. 9. Evolution of a granular packing during compaction $n = 1$, 10, 100 and 1000. The friction coefficient μ is equal to 0.75. Granular mixing is observed due to convection. Indeed, two convection rolls appear in the last picture where the arrows represent the average displacements of the grains during the process.

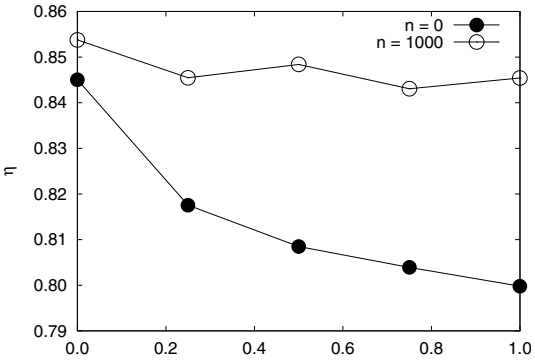

Fig. 10. The initial packing fraction η_0 and the packing fraction after $n = 10^3$ taps as a function of the friction coefficient μ.

Close to the borders, the grains are moving from top to bottom and the grains have an upward motion in the center of the pile.

As presented in Figure 9, the stripes of colored grains are quickly deformed and disappear at the end of the simulation (after $n = 1000$ taps). Convection takes place in the pile for all values of the coefficient of friction. For low friction values, the characteristic time of convection could be higher than the simulation time. Typically, for a coefficient of friction equals to $\mu = 0.5$ or higher, granular convection becomes important and the compaction process is by convection. In order to avoid convection, the simulations were performed periodic boundary conditions and the same aspect ratio of the pile in Figure 9.

The simulations were realized with a limited number of particles ($N = 250$) for efficient simulation runs. Moreover, the periodic boundary conditions limit the finite-size effects due to the small number of grains. Figure 10 presents the evolution of the initial density η_0 as a function of the friction coefficient μ. The case $\mu = 0$ considered here, is an extreme situation which could be encountered experimentally [24]. The initial packing fraction decreases when the friction coefficient increases. The relationship between those variables is strong. This is in agreement with the experimental observations of the previous section.

The compaction process has been computed for five different values of the friction coefficient $\mu = 0.00$, 0.25, 0.50, 0.75 and 1.00. Figure 11 presents typical compaction

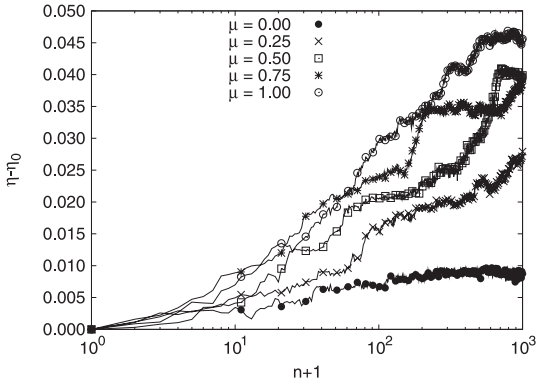

Fig. 11. Five typical compaction curves for different friction coefficients $\mu = 0.00$, 0.25, 0.50, 0.75 and 1.00. The dimensionless acceleration of the pile during each tap is $\Gamma = A\omega^2/g = 6$. We substract the initial packing fraction η_0 in order to obtain curves starting from the same point.

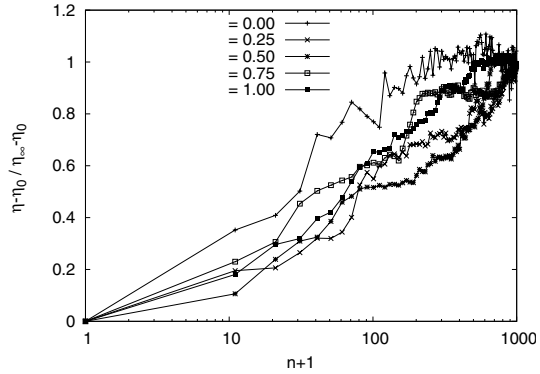

Fig. 12. Normalized volume fraction $(\eta - \eta_0)/(\eta_\infty - \eta_0)$ as a function of n for the five values of the friction coefficient: $\mu = 0.00$, 0.25, 0.50, 0.75 and 1.00.

curves for a dimensionless acceleration $\Gamma = 6$. The frictionless packing has a weak compaction kinetics because the initial packing fraction has a high value. The friction has a strong influence on the initial state which influences the subsequent compaction kinetics. For higher numbers of taps, the compaction kinetics appears to reach the same final state (η_∞) which is independent of the value of the friction coefficient (see white open circles in Fig. 10). The final state depends mainly on grains and tap characteristics. Figure 12 presents the normalized volume fraction as a function of the tap number. The behaviour of compaction for the frictionless case is different from the others ones. For the others values of the friction coefficient no relevant difference appears. The compaction dynamics seems to be unaffected by $\mu > 0$. This result corroborates our experimental data (see Sect. 3.3).

4.3 Numerical challenges

The major limitation of numerical studies is the relative small number of grains. For considering realistic systems like powders, a much larger number of grains is needed. However, the simulation time depends strongly on the

number of particles. Future efforts will be made in order to reach higher numbers of particles in efficient simulation times. This will allow us to consider cohesion in addition of friction in large assemblies.

5 Conclusions

We have experimentally investigated the kinetics of granular compaction. Our analysis shows that this phenomenon is a slow relaxation influenced by microscopic characteristics of the grains. Three important observations have been made :

(i) When a crystallization is observed during the compaction process, the compaction dynamics is better fitted by a stretched exponential law (2). Otherwise, for disordered piles, the compaction dynamics is better fitted by a logarithmic law (1).

(ii) The friction between the grains does not change drastically the characteristic time τ for compaction. However, both initial and final packing fraction values vary strongly with the friction coefficient μ. This result has been confirmed by numerical simulations.

(iii) The cohesion between the grains affects the initial packing fraction value η_0. The cohesion increases the range of accessible packing fraction values $\Delta\eta$ and increases strongly the characteristic time τ for compaction.

Part of this work has been supported by the ARC contract 02/07-293. O.G. would like to thank the Department of Physics, University of Liège for hospitality and support while visiting GRASP where this work was carried out. F.L. thanks the FRIA (Brussels, Belgium) for financial support. We thank J.C. Remy for technical support.

References

1. J.B. Knight, C.G. Fandrich, Chun Ning Lau, H.M. Jaeger, S.R. Nagel, Phys. Rev. E **51**, 3957 (1995)
2. E.R. Nowak, J.B. Knight, E. Ben-Naim, H.M. Jaeger, S.R. Nagel, Phys. Rev. E **57**, 1971 (1998)
3. P. Richard, M. Nicodemi, R. Delannay, P. Ribière, D. Bideau, Nature Materials **4**, 121 (2005)
4. P. Philippe, D. Bideau, Europhys. Lett. **60**, 677 (2002)
5. P. Ribière, P. Richard, D. Bideau, R. Delannay, Eur. Phys. J. E **16**, 415 (2005)
6. F. Ludewig, N. Vandewalle, Eur. Phys. J. E **18**, 367 (2005)
7. E. Caglioti, V. Loreto, H.J. Herrmann, M. Nicodemi, Phys. Rev. Lett. **79**, 1575 (1997)
8. F. Ludewig, S. Dorbolo, N. Vandewalle, Phys. Rev. E **70**, 051304 (2004)
9. G. Lumay, N. Vandewalle, C. Bodson, L. Delattre, O. Gerasimov, Appl. Phys. Lett. **89**, 093505 (2006)
10. T. Boutreux, P.G. de Gennes, Physica A **244**, 59 (1997)
11. G. Lumay, N. Vandewalle, Phys. Rev. Lett. **95**, 028002 (2005)
12. G. Lumay, N. Vandewalle, Phys. Rev. E **74**, 021301 (2006); N. Vandewalle, S. Galam, M. Kramer, Eur. Phys. J. B **14**, 407 (2000)
13. G. Lumay, N. Vandewalle, Phys. Rev. E **70**, 051314 (2004)
14. F.X. Villarruel, B.E. Lauderdale, D.M. Mueth, H.M. Jaeger, Phys. Rev. E **61**, 6914 (2000)
15. A.W. Alexander, B. Chaudhuri, A. Faqih, F.J. Muzzio, C. Davies, M.S. Tomassonea, Powder Technology **164**, 13 (2006)
16. P. Philippe, D. Bideau, Phys. Rev. E **63**, 051304 (2001)
17. S. Remond, Physica A **329**, 127 (2003)
18. F. Radjai, L. Brendel, S. Roux, Phys. Rev. E **54**, 861 (1996)
19. A.V. Tkachenko, T.A. Witten, Phys. Rev. E **60**, 687 (1999)
20. L.E. Silbert, D. Ertas, G.S. Grest, T.C. Halsey, D. Levine, Phys. Rev. E **65**, 031304 (2002)
21. C. Fusco, A. Fasolino, P. Gallo, A. Petri, M. Rovere, Phys. Rev. E **66**, 031301 (2002)
22. M. Renouf, D. Bonamy, F. Dubois, P. Alart, Phys. Fluids **17**, 103303 (2005)
23. M. Renouf, F. Dubois, P. Alart, J. Comp. Appl. Math. **168**, 395 (2004)
24. Y. Bertho, C. Becco, N. Vandewalle, Phys. Rev. E **73**, 056309 (2006)
25. P. Philippe, *Étude théorique et expérimentale de la densification des milieux granulaires*, Ph.D. thesis, Université de Rennes 1, (2002)
26. M. Abramovitz, I. Stegun, *Handbook of Mathematical Functions* (Dover, New York, 1972)